Ship Wave-Induced Hydraulic Loading on Estuarine Groins: a Conceptual Numerical Study

León-Carlos Dempwolff *[1], Christian Windt[1], Gregor Melling[2], Hans Bihs[3], Ingrid Holzwarth[2], and Nils Goseberg[1,4]

[1]Leichtweiß-Institute for Hydraulic Engineering and Water Resources, Technische Universität Braunschweig
[2]Federal Waterways Engineering and Research Institute (BAW)
[3]Norwegian University of Science and Technology (NTNU)
[4]Coastal Research Center, Joint Research Facility of Leibniz Universität Hannover and Technische Universität Braunschweig

Journal of Waterway, Port, Coastal and Ocean Engineering, 2023, **149** 3
DOI: http://dx.doi.org/10.1061/JWPED5.WWENG-1937

Abstract

River training structures, such as groins/spur-dikes, are subject to intensifying ship-induced loads, due to increasing ship dimensions and traffic density on waterways. Especially the long-period primary wave system differs from other loading components such as short-period wind waves due to the long wave length. To date, this loading scenario is not reflected within the empirical based design approaches for groins.

In this study, numerical approaches based on shallow-water theory and CFD are employed for deriving groin design parameters, particularly by assuming stationary load conditions. First, the numerical tools REEF3D::CFD and REEF3D::SFLOW are validated for the specific parameter range of ship-induced groin overtopping based off an experimental data set. Secondly, numerical simulations at prototype scale are connected with empirical equations for armour layer design. Comparing the results to field data from groin prototypes indicates that the combined approach yields plausible required armour layer dimensions. Further, the examination of geometric variations of groins confirms that a reduction of groin slope can reduce the required armour layer dimensions by approximately 10 %.

*Corresponding author,l.dempwolff@tu-braunschweig.de

Introduction

Motivation

In the light of ongoing climate change, river runoff characteristics and associated navigation conditions in rivers and estuaries change significantly. The hydrological impact of a globally rising temperature is of large spatial variance, and a high probability exists to lead to higher river discharge in higher latitudes and lower discharge in the lower latitudes (Nijssen et al., 2001; Hirabayashi et al., 2013); however, findings indicate that total river runoff will likely increase (Labat et al., 2004). At the same time, the temporal variance of river runoff increases, leading to higher flood water levels and lower drought water levels (Arnell, 1999). In that context, river training measures, such as groins, are intended to limit the effect of seasonal variations of discharge and water level with the overall aim to ensure reliable navigation conditions (Alauddin and Tsujimoto, 2012; Remo et al., 2009; Han et al., 2017).

Groins in rivers and estuaries have distinct benefits, specifically in in low water conditions, while only slightly affecting the flow regime during high water conditions. This makes the installation of river groins a widely employed solution in estuarine and river management (Przedwojski, 1995; Sukhodolov, 2014; Alauddin et al., 2017).

Groins limit the effective width (or cross-section) of rivers at mean and low discharge conditions. As a consequence, flow velocities are increased in the river mid-section, while groin arrangement is usually chosen, such that a reduction in flow velocities is obtained near the banks (Alauddin and Tsujimoto, 2012). The accelerated flow increases the erosive potential in the river mid-section ensuring higher navigable water depths along the thalweg than would naturally occur and, therefore, contributes to reliable navigation conditions (Vischer and Huber, 2002; Sukhodolov et al., 2004; Uijttewaal, 2005*a*). The reduction of flow velocities near the banks and sedimentation in the groin fields can reduce the need for protection measures along the banks. This serves to stabilise the course of the river and any horizontal movement or meandering is suppressed. Additionally, the provision of shallow and protected areas in between groins can contribute to the ecological value of a river (Habersack and Nachtnebel, 1995; Schwartz and Kozerski, 2003; Engelhardt et al., 2004; Xiang et al., 2020).

At high discharge conditions, leading to flood events, any restrictions of the waterway cross-section have a potentially negative effect, as higher water levels increase the damage potential of flood events. That means that groins can increase the water level during flood, increasing the damage potential of such events (van Stokkom et al., 2005; Huthoff et al., 2013). In the context of the challenges imposed through climate change and the associated variability of discharge conditions, the installation of carefully designed groins are nonetheless considered a well-balanced tool, leading to larger navigable depths during droughts, while only slightly increasing the damage risk during flood events.

Despite the knowledge documented in the literature pertaining to the erosion of estuarine and river embankments as a result of discharge-related sediment transport, there is astonishingly little work where the effects of ship-waves on embankments or river training structures is discussed.

Findings from the Elbe estuary in Germany suggest that groins along the waterway are damaged due to the characteristic load of ship-generated primary waves (Melling et al., 2019). Ships generate a unique wave system depending on ship and waterway parameters, as outlined in the authors' previous review work (Dempwolff et al., 2022*b*). The main parameters affecting the ship-induced loads are the relation of the ship cross-section to the waterway cross-section (blockage-ratio), the distance between sailing line and the embankment, and the ship speed. Ships with a large submerged cross-section (breadth, draught), such as many modern container vessels that navigate through restricted waterways, generate a notable long-period primary wave. The dimensions of sea-ships make the

associated wave field often times more damaging and therefore design relevant in estuaries, compared to ships designed for inland traffic. The wave length corresponds to the ship length and therefore exhibits lengths of up to 400 m and typical wave periods of 60 s to 120 s, both orders of magnitude longer than naturally occurring wind-generated waves. Moreover, these ship-induced loads typically increase towards the inner estuary as the waterway's cross-section reduces (Finkl and Makowski, 2019), thus introducing large loads to previously sheltered areas. Consequently, sea-ships navigating through estuarine waterways have changed the loads acting in these environments both qualitatively and quantitatively.

The primary ship-wave system comprises several elements. The flow field surrounding the ship has two stagnation points at the bow and stern of the ship. As a result of the low velocities, two water level elevations, known as bow and stern wave, develop at these locations. Between the bow and stern wave, along the ship hull, the accelerated flow leads to a water level depression, also known as drawdown (Bhowmik et al., 1981; Bertram, 2012). The superimposed effects of the drawdown and the stern wave are found to be decisive in the loading and damage of river groins at Elbe estuary (Melling et al., 2019).

Detailed analysis of the hydrodynamic processes during a ship passage has revealed the driving mechanisms of groin damage, as described in detail by Melling et al. (2019) and illustrated in Fig. 1. Conceptually, this erosive process initiates when the ship-generated drawdown moves from one groin field to the adjacent one. Looking at a single groin with an upstream and downstream groin field on both sides, the water level in each groin field depends on the relative position of the ship. The bow wave of the primary wave system is typically negligible due to its relatively small amplitude (Melling et al., 2019). Afterwards, the water level in the upstream groin field lowers due to the drawdown (Fig. 1 b)). A flow over the groin crest opposing the ship's motion direction sets in, due to the water level gradient. As the ship progresses to sail, the ambient water level in the upstream groin field restores and the drawdown moves to the downstream groin field. As a result, a compensatory flow in direction of the ship movement sets in (Fig. 1 c)). This drawdown-induced quasi-stationary groin overtopping in direction of the ship motion coincides with the non-stationary stern wave of the ship. This superposition of loads is considered the critical design case for erosion of a groin (Melling et al., 2019). The observed damage focuses on the groin root, where the structure is attached to the embankment, and the rear slope of the structure near the groin crest. An intensified scour, as typically present near the groin heads, was not observed during field studies (Melling et al., 2020).

This study now intentionally focuses on the effect of the quasi-stationary overtopping process alone, as the decisive loading situation for groin design. That means, that the relatively complex time dependent ship-induced water level variations in two adjacent groin fields (as indicated in Fig. 1(a)-(c)), are reduced to a time-independent situation as indicated in Fig. 1 (c)). The authors reason that this time-independent drawdown-induced process needs particular attention prior to further work on additional transient flow settings, comprising the time-dependent variations of the drawdown, as well as the effect of the stern-wave. . The ship-induced stationary overtopping to date is not fully understood and has received less attention in the available literature. Transient overtopping events, considering the entire ship wave system, including the stern wave will be studied in future work.

Groins are commonly made of a core of filter material protected by armour stones. The diameter of the armour stones, the geometry – in particular the slopes – and scour protection measures at the head are known to be decisive for the resistance against hydrodynamic loading. However, design guidance for river groins is scarce (CIRIA, 2007) and ship-induced waves are not yet considered. For one due to the fact that the overtopping loads generated by large ship wave events are not known a priori, but moreover, there has been a very dynamic development of ship sizes that has certainly outpaced

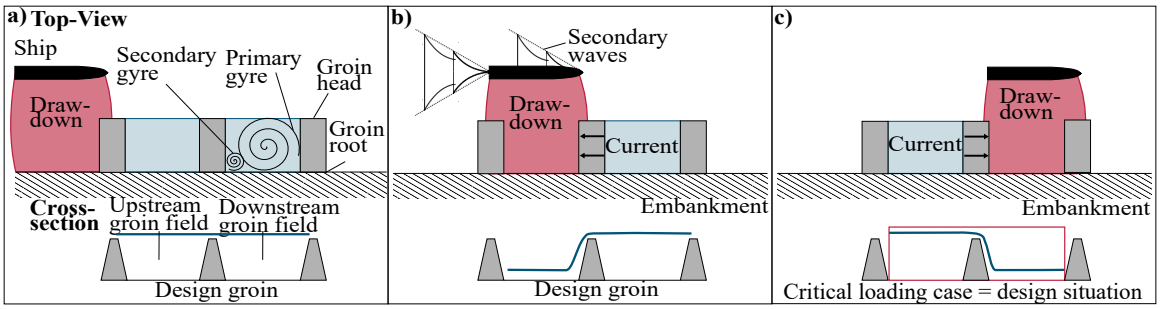

Figure 1: Conceptual sketch of the drawdown induced groin overtopping. **a)** indicates the undisturbed situation before the ship is reaching the design groin **b)** indicates the (beginning) overtopping event opposing the ship's motion direction **c)** indicates the design situation when the drawdown lowers the water level in the downstream groyne field. This water level gradient coincides with the stern wave, therefore highest overtopping loads occur during this time

the development and updates of appropriate guidelines for the protection and suitable design of river training structures. To overcome this limitation, numerical tools can be exploited with significant potential to aid groin design by quantifying the loads from ship-induced overtopping.

Current knowledge

0.0.1 Conventional groin design

Existing studies on the interaction of groins with the ambient river waters have mostly focused on flow phenomena and morphology, often neglecting the stability of groin armour layers. The flow characteristics inside entire groin fields and around individual groins has been intensively researched employing experimental methods, field data, and numerical methods alike (Przedwojski, 1995; Uijttewaal et al., 2001; Minor et al., 2007; Weitbrecht et al., 2008; Sukhodolov, 2014). Taking a 2-dimensional (2D), top-view perspective and looking at flows in a depth-averaged manner, several rotational currents form in between the groins (see also Fig. 1 a)). The momentum exchange between a river and a single groin field induces a primary gyre centrally within the groin field (Tingsanchali and Maheswaran, 1990). Additionally, smaller secondary gyres can develop within the groin field opposing the rotation of the primary gyre (Uijttewaal, 2005*b*; Alauddin et al., 2017).

Scour development due to vertical flow components is emphasized in the research dedicated to groin stability. A pronounced vertical flow component typically forms due to turbulent structures in the mixing layer between the river main stream and the groin field (McCoy et al., 2008; Xiang et al., 2020). In particular near the groin heads and immediately upstream of the groin due to the vertical eddy, the magnitudes of the vertical currents are high, often inducing deep scours (Kuhnle et al., 2002; Alauddin et al., 2017). As these scour holes can critically threaten the overall stability of the respective groin sections, measures to protect the riverbed are usually employed to limit such erosion (CIRIA, 2007). Hence, much of the research attributed to groin stability is seeking to quantify the scour intensity (Garde et al., 1961; Rahman and Muramoto, 1999; Zhang et al., 2018). Studies on the effect of groin arrangement (spacing, length, inclination in respect to main flow) often times rely on numerical models (McCoy et al., 2008; Alauddin and Tsujimoto, 2012, e.g.), while for question of the stability and the design of individual groins, experimental methods are the prevalent approach for design (Kuhnle

et al., 2002; Pandey et al., 2016, e.g.). For further information on groin design and arrangement and their effect compared to other ways to stabilize river streambank see the review of Bigham (2020). Even though Sukhodolov et al. (2004) mentioned the possible influence of navigation on the sediment exchange between groin fields and the main stream, the impact of shipping on the structural stability of groins remains largely unstudied. Often, this lack of knowledge is a direct outcome of the uncertainty that is related to the intricate hydraulics associated with transiently propagating ship waves interacting with geometrically complex river training structures; therefore, the next sub-section reviews current knowledge on this region of interaction.

0.0.2 Determining ship wave loads for structural stability analysis

To date, only few methods are established to consider ship-induced loading in the design waterway infrastructure (e.g BAW (2010)), but these are not specifically applicable to groins. The representation of ship-waves via scaled physical experiments remains very challenging. Ship wave basins can be used to model the entire process cascade from wave generation, wave propagation and wave structure interaction near the embankments (Gourlay, 2001; Lataire and Vantorre, 2008; Rodrigues et al., 2018; BAW, 2018). However, owing to the large size of the critical vessels, only a small model scale is possible (typically between 1:40 to 1:60). At such a small scale, while Froude scaling can be maintained, the turbulent flows in the vicinity of structures are no longer appropriately represented as Reynolds numbers drop below recommended typical values to hold similitude criteria in an appropriate range (Méhauté, 1976; Hughes, 1993).

Other experimental procedures employ flumes, where a sub-set of the parameters relevant for long-period ship waves can be approximated. Silinski et al. (2015) used monochromatic waves with a long period to represent ship waves. However, this only partly reflects the parameter space relevant for real ship waves, as the maximum wave-length of wave makers is typically limited and the directionality as well as the transient nature of the phenomenon is not incorporated at all. Analogies between long-period tsunami waves and ship waves are reported, as both waves originate from mass displacement (Didenkulova et al., 2011). For tsunami wave generation a rich body of literature exists (e.g. Goseberg (2013), von Häfen et al. (2019)) that indicate future research paths to improve experimental methods to represent ship-generated primary waves; however, even these works have not explicitly expressed applicability to ship wave contexts.

Field measurements (Almström et al., 2021; Forlini et al., 2021; Tomiczek et al., 2022) can contribute to process understanding of ship wave propagation and their interaction with embankments, yet these methods do not allow a direct transfer to prognostic methods. In addition, these methods provide very valuable as reference data in the validation of numerical methods to compute ship-generated waves.

Several numerical methods exist, that are able to predict the far-field propagation of ship-generated primary waves. In particular, depth-averaged methods based on Shallow-Water-Equations (SWE) or Boussinesq equations are successfully applied to obtain data on the generation and propagation of ship-generated primary waves. Commonly, a pressure term is included in the free surface of the model, representing a ship hull. This method proved reliable over a large parameter range (Forlini et al., 2021) and in complex bathymetric situations (Almström et al., 2021). Several components of the ship wave system can be computed with such methods, namely the short-period secondary wave system (David et al., 2017), the long-period primary wave system (Almström et al., 2021), and the precursor soliton generated by fast ships (Shi et al., 2018). Yet, some of the complex processes connected to groin overtopping, such as stratified flows, vertical velocity accelerations, and turbulent processes

in the overtopping flow and in particular within the hydraulic jump downstream of the groin, are not covered by the depth-averaged theory (Elsayed et al., 2022). Steep bed level gradients can also limit the application of depth averaged tools, dependent on the exact slope of the bed gradient and the utilized numerical tool (Říha et al., 2019). Therefore numerical models need to be tested carefully to ensure that planned applications lie within the respective model limitations.

Conceptual numerical approach for groin design

Due to these limitations of current experimental and numerical tools, novel modelling approaches are in demand. For example, one may combine high-fidelity simulations near river training structures, e.g., groins, with efficient numerical modelling of ship wave generation and propagation that is efficient for larger computational domains.

The loading situation during quasi-stationary ship-induced overtopping, depends on the water level in adjacent groin fields. The hydraulic head in the upstream groin field itself depends on the ambient water level, that is either controlled by tidal water levels in estuaries or related to riverine water levels based on discharge conditions. The downstream water level depends on the maximum drawdown amplitude, that is mostly controlled by ship parameters, such as the ratio of ship to waterway dimensions (blockage factor), ship speed and the distance in between the sailing line and an embankment. Regarding the ship wave generation and propagation, depth-averaged numerical methods have successfully been applied for calculating the water level time series dependent on ship parameters (David et al., 2017; Almström et al., 2021) and can therefore be applied to inform the groin downstream water level for further simulations of small scale flow details near a groin in the future.

Previous work (BAW, 2018) has suggested that the quasi-stationary flow situation examined in this study, can be approximated by an overtopping weir flow analogy and its well-known design formulae (e.g. Hager (1987); Vanden-Broeck and Keller (1987)). CFD modelling is routinely applied for the design of weirs. Haun et al. (2011); Chen et al. (2018); Jiang et al. (2018); Kamath et al. (2019) used Reynolds-averaged Navier-Stokes equations (RANSE)-based high-fidelity CFD models to quantify the relation of discharge and waterlevel. Depth-averaged models are used to quantify the overflow and free surface profile over weirs. Examples of such applications are presented by Darvishi et al. (2017); Říha et al. (2019) that indicate the accurate performance for the examined flow conditions.

Other structures that exhibit a number of analogies to groins are overtopped levees. Hughes and Nadal (2009) studied the combined effect of wind waves and storm on the specific overflow by means of an experimental set-up. The results indicate, that the overflow of the two contributors can reasonably approximated by an empirical regression equation. Sharp and McAnally (2012) present a numerical twin of Hughes and Nadal (2009)'s experimental set-up with a shallow water equation solver, showing that the employed model *ADH* can indeed deliver an accurate prognosis of the respective velocity data. Empirical equations for the determination of the corresponding shear stress, indicate that the structure is particular susceptible to damage through shear stress peaks at locations of slope transitions and dependent on Manning's roughness coefficients.

Despite the analogies between embankment weirs, overtopped levees and groins, several differences exist with regard to the determining parameter space. While embankment weirs are typically constructed with an upstream slope of 1:1 or 1:2, the slopes of groins are often less steep, up to a value of 1:4. The roughness of the groin surface constructed from rock grading is significantly higher than typical weirs made from concrete. The critical cases when damage is observed are characterized by very low head heights ($h/p_g < 0.5$), where h denotes the hydraulic head and p_g the groin height. At such low hydraulic heads, a significant vertical flow contraction can be expected (Říha et al., 2019),

possibly challenging the application of a SWE tool. Using a non-hydrostatic pressure assumption conserves some of the vertical flow information, therefore presumably improving the performance for low head height, but still careful testing is required. Therefore, a validation of the high-fidelity and depth-averaged numerical models needs to be performed for the relevant parameter space to obtain information on model limitations and consequently evaluate the potential of using the respective model in subtasks connected to adequate design and arrangement of groins.

In this study, experimental data is employed to validate numerical models for the stationary loading situation (Wöffler et al., 2013; BAW, 2018). Even though the transient nature of ship waves is neglected in this approach, the stationary loading situation is a determining sub-component of the complex damage mechanism, highlighted in Section , that needs attention, prior to the examination of the time-dependent loading situation. The hydraulic loading of overtopped structures depends on the water level on each side of the respective construction. During prototype groin overtopping, the downstream water level is determined by the drawdown amplitude. The larger the drawdown, the more intense the flow to overcome the water level gradient. At free flow conditions, no moderating effect from the downstream water level on the overtopping flow is present. From a design perspective, it is therefore desirable to include the free outflow in the studied load cases, as this condition represents the worst case stationary loading scenario, neglecting the additional effect of the stern wave. Hence, the examined load cases in the experimental study and the numerical simulations for validation and the prototype study are based on free weir flow conditions.

Objectives

Consequently, this study seeks to exploit the capabilities of numerical models to determine the hydraulic loading from quasi-stationary ship-induced groin overtopping.

The present article for the first time presents a numerical concept for studying stationary groin overtopping and the influence of geometric variations on groin loads. Two numerical model modules, REEF3D::CFD and REEF3D::SFLOW, are firstly validated for the relevant parameter range, ensuring that the quasi-stationary loading situation is represented accurately. Then, field data providing boundary conditions for critical loading scenarios are identified to inform a numerical case study in prototype scale. The numerically obtained hydrodynamic information is used as input for empirical design equations for rock armour layer (CIRIA, 2007; Thornton et al., 2014). The qualitatively plausible results for the stationary simulations with REEF3D::SFLOW make the numerical code a promising design tool for groins under stationary discharge assumptions. Successful adaptions of the groin design are examined numerically, identifying the effect of geometric variations on required stone classes.

The specific objectives of the present study are hence threefold:

- To validate REEF3D::CFD and REEF3D::SFLOW for stationary overtopping at low head heights and obtain model limitations
- To evaluate the plausibility of the numerically-obtained velocity field for the stationary overtopping concept to describe ship waves in prototype scale, using field data as boundary conditions
- To examine the sensitivity of groin loading to field-tested geometric variations of the design (rounding the crest, employing a more gentle slope)

These goals are a stepping stone towards a future coupled simulation tool making use of the efficiency of shallow water theory while maintaining high-accuracy in vicinity to groins. The

REEF3D modelling family (Wang et al., 2020*a*) provides solvers for both, high-fidelity modelling (REEF3D::CFD) (Bihs et al., 2016) and depth-averaged modelling (REEF3D::SFLOW) (Wang et al., 2020*b*). An inclusion of ship representation in REEF3D::SFLOW has recently been implemented. A series of verification tests shows that the adapted model functionalities can indeed be employed to represent ship-generated waves (Dempwolff et al., 2022*a*). These solvers will therefore be applied in the combined modelling tool.

The remainder of this paper is structured as follows. The numerical methods and the experimental set-up used for their validation, as well as the the empirical approaches for armour layer design are given in Section 0.0.2. Results are presented in Section 0.0.4. This section comprises the results of the validation in Section 0.0.4 and the prototype showcase study results in Section 0.0.6. This is followed by a discussion in Section 0.0.6, discussing both validation and the prototype study results. Finally, concluding remarks and future work are presented in Section 0.0.6.

Materials and Methods

The analysis presented in Section 0.0.4 relies on numerical tools, validation data, and empirical equations for armour layer dimensioning. In order to provide the necessary background information for the interpretation of the results, the governing equations of the employed models are introduced in the following Section 0.0.2. The experimental procedure for obtaining validation data is presented in Section 0.0.4. The empirical equations and the parameters present at the example site are then introduced in Section 0.0.4.

Numerical methods

0.0.3 REEF3D::CFD

REEF3D::CFD is a hydrodynamic solver based on the RANSE, describing the conservation of mass:

$$\frac{\partial u_i}{\partial x_i} = 0, \tag{1}$$

and the conservation of momentum:

$$\frac{\partial u_i}{\partial t} + u_j \frac{\partial u_i}{\partial x_j} = -\frac{1}{\rho}\frac{\partial p}{\partial x_i} + \frac{\partial}{\partial x_j}\left[(\nu + \nu_t)\left(\frac{\partial u_i}{\partial x_j} + \frac{\partial u_j}{\partial x_i}\right)\right] + g_i. \tag{2}$$

Parameter x_i denotes the coordinates in x, y, z-directions and u_i denotes the velocity vector. The time is given by t, the pressure by p. Parameter ν and ν_t are the kinematic and turbulent viscosity, respectively. ρ denotes the fluid density, and g the acceleration due to gravity.

The free surface is described by a level-set function describing the distance to the free surface. Solid boundaries are accounted for using a ghost cell immersed boundary approach, extrapolating the solution into solid regions. High-order discretisation schemes are used, such as the fifth-order WENO scheme for the convective terms and a third order accurate TVD Runge-Kutta scheme for time treatment of the momentum and level set equations. The discretisation in time is further based on an adaptive time-stepping criterion. The user input for the CFL-criterion determines the time step dt, considering the grid size and maximum velocities within the domain.

Due to the employment of the complete RANSE, viscous three dimensional processes can be quantified with a high level of detail. The solver found wide application in numerous applications

focusing on wave propagation (Kamath et al., 2017), fluid-structure interaction (Aggarwal et al., 2020) and open channel flow (Afzal et al., 2020). Additional features include floating body-fluid interaction (Martin et al., 2021), the determination of morphological activities (Ahmad et al., 2019), and mooring dynamics (Martin et al., 2020). Efficient parallelisation using the open Message Passing Interface (MPI) protocol allows the use of a large number of processors reducing the required computational time. Due to the solution in three spatial dimensions and the required high mesh resolution the computations are still very resource-demanding, as further discussed in Section 0.0.6.

0.0.4 REEF3D::SFLOW

REEF3D::SFLOW is a shallow water equations solver (Wang et al., 2020*b*). The inherent model assumptions limit the module to cases where the characteristic horizontal length scale (wave length) is large compared to the determining vertical dimensions (water-depth) and no steep-bed gradients exist. The reason is that vertical velocity components are simplified, therefore model configurations that require an accurate determination in this dimension can not be reliably predicted. However, for many coastal and estuarine areas, the model assumptions are appropriate, so that the fast simulation times of large domains is a significant benefit over any accuracy concern, leading to the application of shallow water theory in various cases (Roelvink et al., 2009; Zijlema et al., 2011). In close vicinity to groins, pronounced variations in the water depth exist and hydrodynamic structure interactions set in. This presumably leads to pronounced vertical velocity components or accelerations, possibly limiting the applicability of shallow water theory.

Compared to other depth-averaged numerical models REEF3D::SFLOW has several advantages. The pressure is included in its non-hydrostatic form, as suggested by Jeschke et al. (2017). This allows an inclusion of a depth-averaged vertical velocity component, leading to a more accurate description of the dispersion characteristics of waves. Therefore, relatively short waves can still be calculated by REEF3D::SFLOW. At the same time, only one vertical flow layer is included and the code is efficiently parallelized, leading to very fast calculations. The governing equations rely on the depth-averaged mass and momentum equation with the non-hydrostatic pressure extension by Jeschke et al. (2017):

$$\frac{\partial \zeta}{\partial t} + \frac{\partial h_S \bar{u}}{\partial x} + \frac{\partial h_S \bar{v}}{\partial y} = 0, \tag{3}$$

$$\frac{\partial \bar{u}}{\partial t} + \bar{u}\frac{\partial \bar{u}}{\partial x} + \bar{v}\frac{\partial \bar{u}}{\partial y} = -g\frac{\partial \zeta}{\partial x} - \frac{1}{\rho h_S}\left(\frac{\partial h_S q}{\partial x} - \left(\frac{3}{2}q + \frac{1}{4}\rho h_S \phi_{nh_S}\right)\frac{\partial d}{\partial x}\right), \tag{4}$$

$$\frac{\partial \bar{v}}{\partial t} + \bar{u}\frac{\partial \bar{v}}{\partial x} + \bar{v}\frac{\partial \bar{v}}{\partial y} = -g\frac{\partial \zeta}{\partial y} - \frac{1}{\rho h_S}\left(\frac{\partial h_S q}{\partial y} - \left(\frac{3}{2}q + \frac{1}{4}\rho h_S \phi_{nh_S}\right)\frac{\partial d}{\partial y}\right), \tag{5}$$

$$\frac{\partial \bar{w}}{\partial t} + \bar{u}\frac{\partial \bar{w}}{\partial x} + \bar{v}\frac{\partial \bar{w}}{\partial y} = -\frac{1}{\rho h_S} - \left(\frac{3}{2}q + \frac{1}{4}\rho h_S \phi_{nh_S}\right), \tag{6}$$

Here, $\bar{u}, \bar{v}, \bar{w}$ are the depth-averaged velocity components in x, y, z-direction. $\bar{p}$ is the depth-averaged pressure, d is the still water depth and ζ is the free surface elevation and $h_S = d + \zeta$. The term $\frac{3}{2}q + \frac{1}{4}\rho h \phi_{nh}$ denotes the quadratic vertical pressure profile (Jeschke et al., 2017).

For further details of the model implementation and its application compared to the REEF3D::CFD module see (Wang et al., 2020*b*,*a*).

Table 1: Hydraulic heads and associated discharges further studied in the numerical simulations (the experimental data encompasses higher hydraulic heads as well)

Case #	hydraulic head h [cm]	discharge q [m^2/s]	h/p_g [-]
1	2	0.0054	0.154
2	3	0.0095	0.231
3	7	0.032	0.538

Experimental examination of the relation between water level and discharge

An experimental test campaign was conducted to quantify the ship-induced loads on groins. To date, no generally accepted experimental procedure is established, that represents the entire complex interaction processes of river training structures with long-period ship waves. Therefore, simplified model assumptions need to be introduced to partly reproduce features of the ship wave system. Following our conceptual description of groin overtopping induced by different ambient water level in adjacent groin fields, a simple stationary model is chosen (see also Wöffler et al. (2013),BAW (2018)). This experimental arrangement depicts the drawdown induced overtopping event, as depicted in Figure 1 (c), while subsequent transient events (stern-wave) are neglected.

The experimental set-up is depicted in Fig. 2. It replicates the situation as shown in Figure 1 c). The scaled groin consists of a gentle and constant wave-facing slope, a flat groin crest, followed by a decreasing lee-side slope. A homogeneous groin cross-section was installed in a 1 m wide and 30 m long current flume at the experimental facilities of the institute for hydraulic engineering and water resources management (IWW) at RWTH Aachen, Germany, without a bed gradient. A pump provided constant discharge (frequency-controlled) upstream, so that a stationary hydraulic head h set in on the upstream side of the groin model. The discharge was chosen iteratively to establish the head heights given in Tab. 1.

Water levels were measured at five locations using Microsonic ultrasonic wave gauges *mic+35*, with an accuracy of +/- 1 %, a sensing range between 65 mm to 600 mm, and a sampling frequency of 20 Hz. The position of the gauges is included in Fig. 2. Resulting water levels were time-averaged over the entire time series to neglect the impact of small scale surface perturbations. The water level at these gauges is evaluated for the model validation and will be compared to the numerical results.

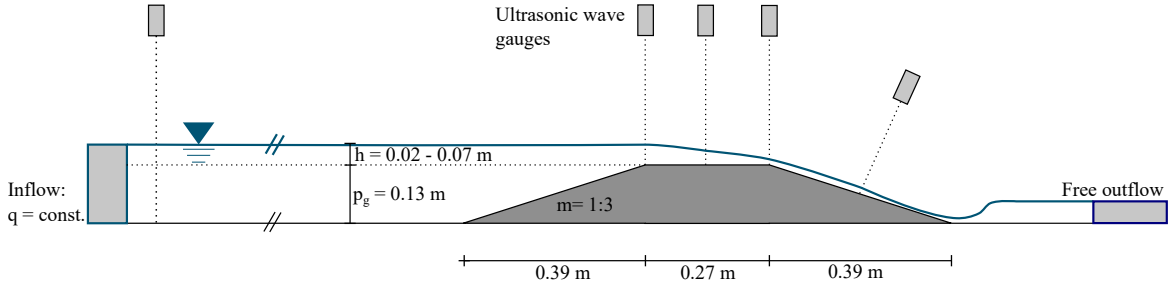

Figure 2: Experimental set-up and the respective gauge locations.

Empirical equations for rock armour layer

The dimensioning of rock armour layer is decisive for the design of a large range of coastal structures including riprap embankments, breakwaters, and rockfill dams. Hence, a variety of empirically–based equations has been suggested, derived for specific loading scenarios, e.g., short period wind waves and storm surges (Hudson, 1959; van der Meer, 1987; Van Gent et al., 2004; EurOtop, 2018). However, these are not applicable to primary ship waves, as the associated overtopping process exhibits a long period, rather resembling a non-transient problem, as indicated in Figure 1 c). Therefore, two general equations intended to be used for stationary, unidirectional flow situations were employed in this study.

The first equation considered is that of Thornton et al. (2014) which relies on a meta analysis of existing studies and equations on riprap design. These authors suggest a regression formula that allows the determination of armour layer dimensions dependent on the specific discharge as given in Eq. (7).

$$D_{50} = 0.575 S^{0.2} C_u^{0.28} q^{0.21} t^{0.62} [1.16/(SG-1)^{0.30}] \tag{7}$$

Here, S is the slope of the construction assumed to correspond to the respective groin lee slope. The remaining parameters are chosen as: the coefficient of uniformity $C_u = 3$, the armour layer thickness $T = 2 \cdot D_{50}$, stone density $\rho_s = 3700\,\mathrm{kg/m^3}$, the Nikuradse roughness length $k_s = 4 \cdot D_{50} = 0.88\,\mathrm{m}$. SG is defined as $\frac{\rho_s}{\rho}$.

The second approach is the commonly used shear stress-concept of Shields, here reprinted following CIRIA (2007). The equation relies on the velocity and water-depth to determine adequate armour layer dimensions and is applicable for armour layer dimensions $D_{50} > 0.064\,\mathrm{m}$ CIRIA (2007). The governing equation is given in Eq. (8). The determination of required armour layer depends on the appropriate choice of the Shields parameter, ψ_{cr}, which can be chosen between 0.03 and 0.055. Within this interval, 0.03 corresponds to no movement at all, while at 0.055 some limited stone movement already sets in. Due to the high frequency of the load events, a small value of 0.035 is chosen in this study.

$$\psi_{cr} = \frac{1}{C^2} \cdot \frac{U_{cr}}{\Delta D k_{sl}} \tag{8}$$

with:

$$C = 18 log(1 + 12d/k_s) \tag{9}$$

Here, U_{cr} is the critical depth-averaged velocity, Δ is the relative buoyant density, and D is the characteristic stone diameter, typically equal to median sieve size D_{50}. Parameter k_{sl} is the slope reduction factor, taking into account the reduced stability of armour layer on sloped surfaces. The equation includes the structure slope angle, β, and the angle of repose of the armour layer, ψ, according to Eq. (10) (CIRIA, 2007).

$$k_{sl} = \frac{\psi - \beta}{\phi} \tag{10}$$

Results

Based on the presented methods, results in two different scales were obtained. Firstly, numerical model set-ups according to the experimental procedure presented in Section 0.0.4 were established. These were used to validate the presented numerical methods REEF3D::CFD and REEF3D::SFLOW for

the critical parameter range of ship-induced overtopping events (Section 0.0.4). After validating the accuracy of the numerical codes, a case study, based on the previously established model configurations and informed by field data, is presented in Section 0.0.6. This case study pursues to examine if the resulting velocity fields of the numerical simulations for the stationary loading situation are within a plausible range and to study the effect of different geometric variations of groin construction.

Validation for low hydraulic heads

0.0.5 Numerical model set-up and error margins

The numerical model set-up is outlined in the following. For a visual representation see Fig. 3. In both numerical models, REEF3D::SFLOW and REEF3D::CFD, two-dimensional slice models of the experimental set-up are employed (i.e., the x-z-plain), to save computation time. Symmetry planes in lateral direction ensure no additional energy dissipation due to the 2D assumption. The CFD simulations use a $k-\omega$-turbulence model, an extensively validated standard option of REEF3D::CFD (e.g. Bihs et al. (2016); Kamath et al. (2019)), while the REEF3D::SFLOW simulations do not make use of a turbulence model. The boundary conditions perpendicular to the flow directions are chosen according to the experimental set-up. Initially a constant water level in the entire domain is assumed.

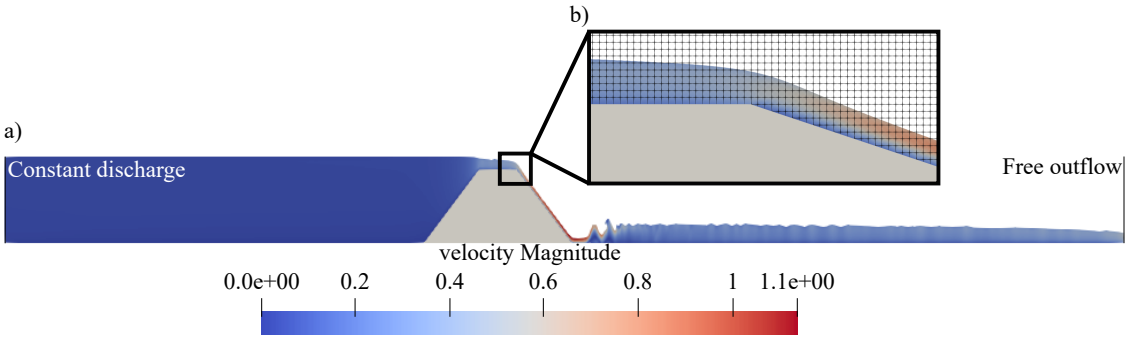

Figure 3: a) Numerical modelling set-up for stationary flow situation; depicted for REEF3D::CFD and scaled with a factor of 4 in vertical direction b) employed computational mesh resolution of $dx = 0.0025$ m.

A stationary flow situation is ensured, by analysing time series of the different water level gauges in the domain. If the water level at each of the gauges is constant (standard deviation was below 0.001 m), the values for the gauges were extracted and used for further data processing. As an example, for the procedure to identify the stationary state see the time histories in the appendix (Fig. 11).

The accuracy of the computational simulation, tied to the employed mesh resolution, was determined by means of a convergence study. The employed method relies on an extrapolation procedure as suggested by Viola et al. (2013). In the present study, the case with the smallest hydraulic head of $h = 2$ cm was employed to examine model convergence. Results for the water level at the first gauge are computed for meshes of varying resolution and extrapolated to an continuous solution, as presented in the appendix (Fig. 9 and 10).

For the REEF3D::CFD simulations a mesh was chosen depending on the hydraulic head of the respective simulation. A mesh resolution of $h/dx = 8$ was found to provide a good compromise between accuracy and efficiency compared to resolutions of $h/dx = 4$ an $h/dx = 16$. Here dx denotes the size of the square cells. At this resolution an acceptable discretisation error of 0.39 % was identified.

The resolution for REEF3D::SFLOW can be chosen significantly coarser than for the REEF3D::CFD simulations. A mesh of $dx = 1$ cm was identified as sufficient. The convergence error at this resolution is 0.15 ‰ for the case with a hydraulic head of 2 cm. The domain consist of a single vertical layer, as the underlying equations allow an non-hydrostatic approach without introducing additional vertical layers (see Section 0.0.4). Therefore, no dependency of the hydraulic head and the mesh resolution could be included. A summary of the chosen discretisation and resulting parameters is given in Tab. 2.

For time discretisation, no influence of the CFL-criterion on the solution from both CFD and SFLOW was found. Therefore, a relatively high value for $CFL = 0.75$ was chosen as an adaptive time-stepping criterion.

Table 2: Numerical discretisation meshes used for further simulations and associated parameters

Solver	Cell number	$[h/dx]$	dx	Comp. time	Processors	Error
CFD	640,000	8	0.25 cm	17.6 h	32 à 2.35 Ghz	0.39 ‰
SFLOW	800	depth-averaged	1 cm	78 s	8 à 2.35 Ghz	0.15 ‰

0.0.6 Validation study results

Fig. 4 show results of the free surface level along the domain for REEF3D::SFLOW and CFD together with experimental data. The qualitative results indicate an overall reliable prediction of the water level with both numerical models. The hydraulic head, as well as the drop in water level at the position of the groin are calculated accurately. Both models slightly overpredict the water level throughout the domain.

The largest differences between the results of REEF3D::SFLOW and REEF3D::CFD are present in the downstream region of the groin. Here, a hydraulic jump occurs when the flow regime is shifting from supercritical to subcritical. The associated increase in flow depth is predicted by REEF3D::SFLOW. However, fluctuations in the free surface due to the vertical velocity components expected at the location of the jump cannot be predicted. The REEF3D::CFD module predicts these small scale flow processes qualitatively well. Yet, the experimental data as described Section 0.0.4 do not include any information on the hydraulic jump, such that no detailed analysis is possible. This is due to the overall scope of this work, where the overflow portion over the structure was in primary focus.

Quantitative results of the accuracy of the numerical results presented in Fig. 5 further highlight the reliable calculation of the water level for the considered parameter space. The quantification of the deviations between numerical and experimental data relies on the Mean Absolute Percentage Error (MAPE). This error metric was calculated for each test, according to:

$$MAPE = \frac{100}{N} * \sum_{i=1}^{N} \left| \frac{R_m - R_s}{R_m} \right|, \tag{11}$$

where N is the number of samples, R_m is the experimentally determined water level at each specific gauge and R_s is the numerical value at the respective gauge.

The error bars in Fig. 5 depict the combined uncertainties from the measurement inaccuracies ($+/-1$ ‰), and the grid uncertainty as summarized in Tab. 2. Not included are possible errors from the discharge measurements in the experimental tests. The results indicate the reliability of the

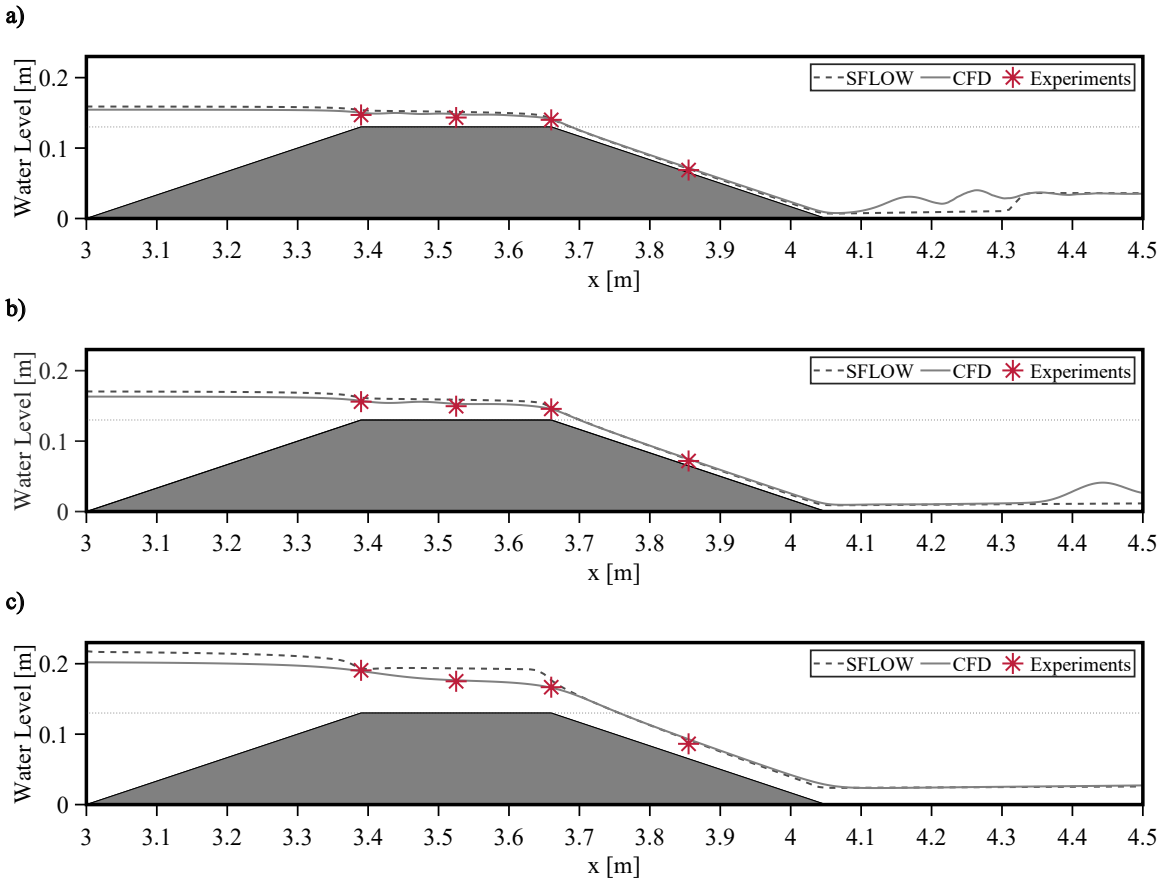

Figure 4: Free-surface profiles for all cases a) case #1 ($q = 5.4 * 10^{-3} m^2/s$; b) case #2 ($q = 9.5 * 10^{-3} m^2/s$); c) case #3 ($q = 3.2 * 10^{-2} m^2/s$).

numerical tools with a maximum MAPE of <3 % for the REEF3D::CFD module and <7 % for the REEF3D::SFLOW module.

The error resulting from the REEF3D::CFD simulations is notably smaller than for the REEF3D::SFLOW simulations and decreases with increasing hydraulic head. On the contrary, the error from the REEF3D::SFLOW simulations increase with increasing hydraulic head. It can be hypothesized that the steeper water level gradients occurring at higher discharge conditions lead to this observation. However, even the maximum error resulting from REEF3D::SFLOW is still within an acceptable range. Even for the small domains of the presented 2D-simulations REEF3D::SFLOW is several orders of magnitude faster (e.g around 350 times for case #1) than REEF3D::CFD. Both models can hence be considered valid simulation tools for stationary overtopping of groins with low hydraulic heads.

Case study for prototype groin using field data

To determine hydraulic processes on a prototype groin scale, additional simulations are performed, where the input boundary conditions are based on field data. In the field, an adapted groin design was tested at the Elbe estuary, Germany, to limit the damaging effect of ship-induced overtopping (Melling et al., 2020). The groin field is geo-located at E 9.567°, N 53.616°. The location of the groin field in

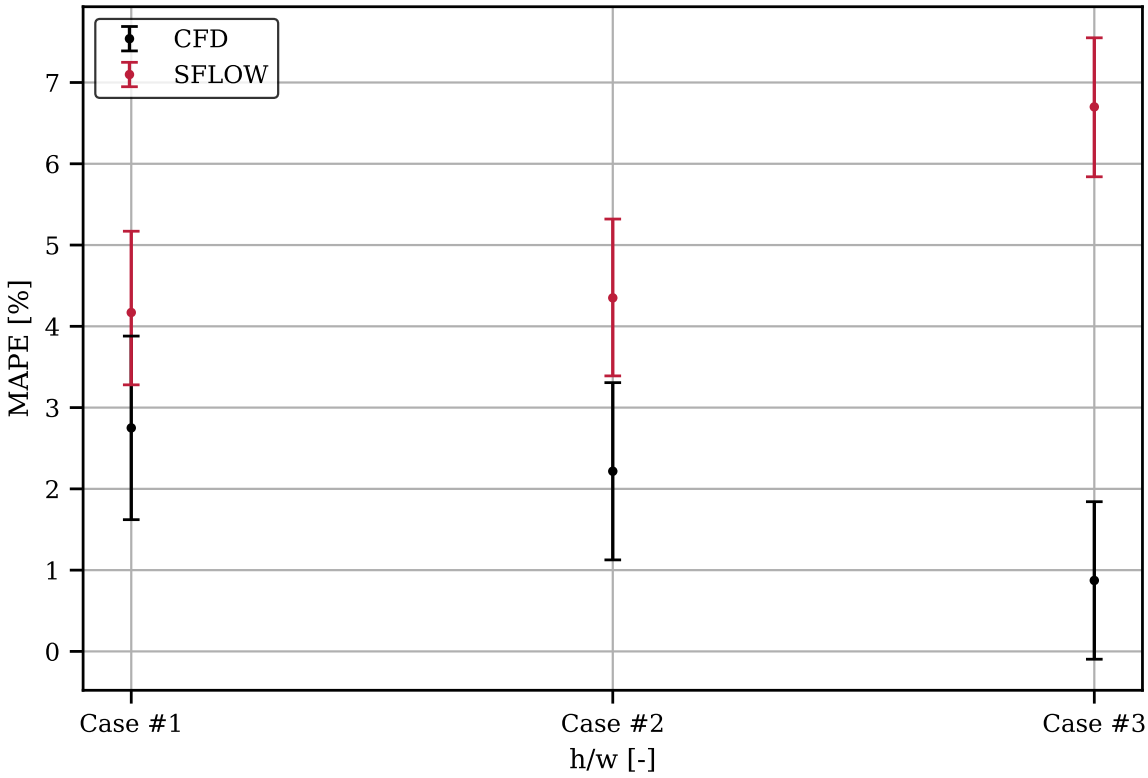

Figure 5: MAPE between the numerical and experimental results for the considered test cases

respect to the Port of Hamburg is depicted in Fig. 6 a). A detailed view on parts of the groin field is shown in Fig. 6 b).

During a monitoring campaign it was revealed that the adapted design was less prone to damage due to primary waves (Melling et al., 2020). However, several design parameters were adapted simultaneously, such that an evaluation of the contribution of specific design changes to the increased stability is not possible. Therefore, the changes, that can be represented in a slice model, are incorporated in a numerical parameter study to showcase the application of the previously validated model REEF3D::SFLOW in the design process of groins. The measurements indicate critical overtopping events with $h = 0.75\,\mathrm{m}$. At the prototype groin scale present in the Elbe estuary this corresponds to $h/p_g = 0.25$. The numerically obtained hydrodynamic information is used as input data to empirically based design equations (see Section 0.0.4) to derive an estimation of necessary armour layer design.

The adapted design incorporates three modifications (see also Fig. 7): (i) A reduction of the slope angle (1:4 instead of 1:3) (ii) Rounding the groin crest removing any sharp transitions. (iii) Using a stone class with a higher mean diameter and weight. In the conventional design the grading $CP_{90/250}$, corresponding to a median diameter of $D_{50} = 0.125\,\mathrm{m}$, (CIRIA, 2007) was applied. In the adapted design, the grading $LMB_{5/40}$ was used. As this stone class is defined by its weight instead of geometric parameters, a range of plausible diameters exists. In this study, a median sieve size D_{50} of $0.22\,\mathrm{m}$ is considered for the further examination. (i) and (ii) were included in the numerical simulations, while (iii) was considered in the evaluation of the required stone dimensions. For an overview of the resulting geometries tested see Tab. 3.

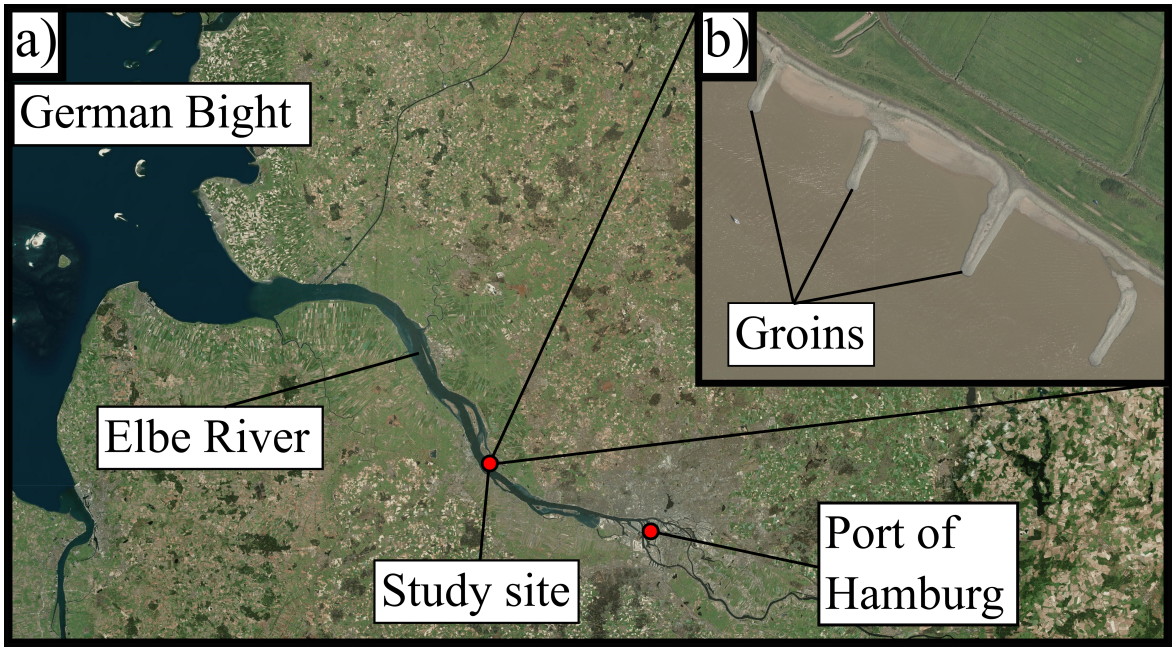

Figure 6: a) Location of the study site in respect to the river reach; b) aerial image of the groin field examined in the case study (Image Source: WSV (2016))

Table 3: Geometric configurations tested in the showcase study with REEF3D::SFLOW

Abbreviation	Slope	Crest design
F33	Both: 1:3	Flat
F44	Both: 1:4	Flat
F34	Luv: 1:3; Lee: 1:4	Flat
R33	Both: 1:3	Rounded
R44	Both: 1:4	Rounded

The hydrodynamic information obtained from the numerical model is connected to information on groin stability via two empirical approaches for the determination of required stone classes (Section 0.0.4). The numerical results were used to calculate the missing parameters required for the application of the empirical equations, such as the specific discharge and the local velocity field. Quantities such as the discharge over the groin are difficult to measure in the field. Using a numerical simulation to predict the relation of water level to discharge is hence a way to determine adequate armour layer dimensions relying only on water surface measurements and to avoid more complex field campaigns including discharge measurements.

Qualitative results of the flow velocity and water level obtained with REEF3D::SFLOW for the groin in prototype scale are given in Fig. 8 a) for the conventional design and in Fig. 8 b) for the adapted design. Even though the discharge is constant throughout the entire domain, critical processes only set in on the lee slope of the groin according to the Shields equation. At the lee slope, the flow velocities are high, while the flow depth is low. Therefore large stone diameters are required here, but

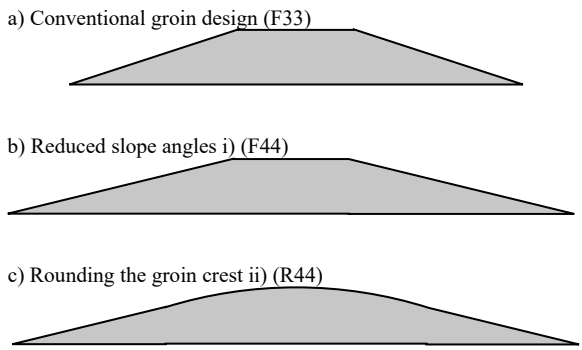

Figure 7: Cross section of different groin geometries; a) shows the conventional groin design b) indicates more gentle slopes and c) indicates gentle slopes and a rounding of the crest

still the maximum velocity is lower than the critical velocity, indicating that no erosion takes place. This indicates that, for the given armour layer dimension of $D_{50} = 0.22\,\mathrm{m}$, the groin proves stable under stationary discharge conditions.

Quantitative results on the effect of the construction parameters on the required armour layer dimensions to resist the drawdown-induced overtopping are summarized in Tab. 4.

The results of the empirical equation of Thornton et al. (2014) are constant throughout the domain as they only rely on the discharge. The resulting armour layer dimensions are in good agreement with the maximal value indicated by the Shields equation, therefore establishing some further confidence in the numerical approach.

Table 4: Results from the numerical simulations with REEF3D::SFLOW at different geometric configurations

Result	Base Case F33	F44	F34	R33	R44
$u_{max}[m/s]$	5.22	5.03	5.03	5.14	5.08
$D_{50}[m](Thornton)$	0.178	0.159	0.159	0.171	0.160
$D_{50}[m](Shields)$	0.160	0.125	0.125	0.165	0.122

Discussion

Both numerical models, the RANSE-based model REEF3D::CFD and the SWE-solver REEF3D::SFLOW, predict the relation of discharge and water surface elevation qualitatively well with a MAPE below 7 %. Even though the error margin of the REEF3D::CFD module is smaller than that of REEF3D::SFLOW, the accuracy of REEF3D::SFLOW is still deemed appropriate for most engineering applications. The increased accuracy of the CFD module comes with significantly higher computational costs.

The 2D-slice model only partly represents this advantage, due to the small model domain. More precise simulations specific to local conditions will require including details of the local bathymetry. In particular, this is the beach slope orthogonal to the groin axis. Numerical simulations including these details will incorporate significantly larger domains. While this is not a problem for the cost-

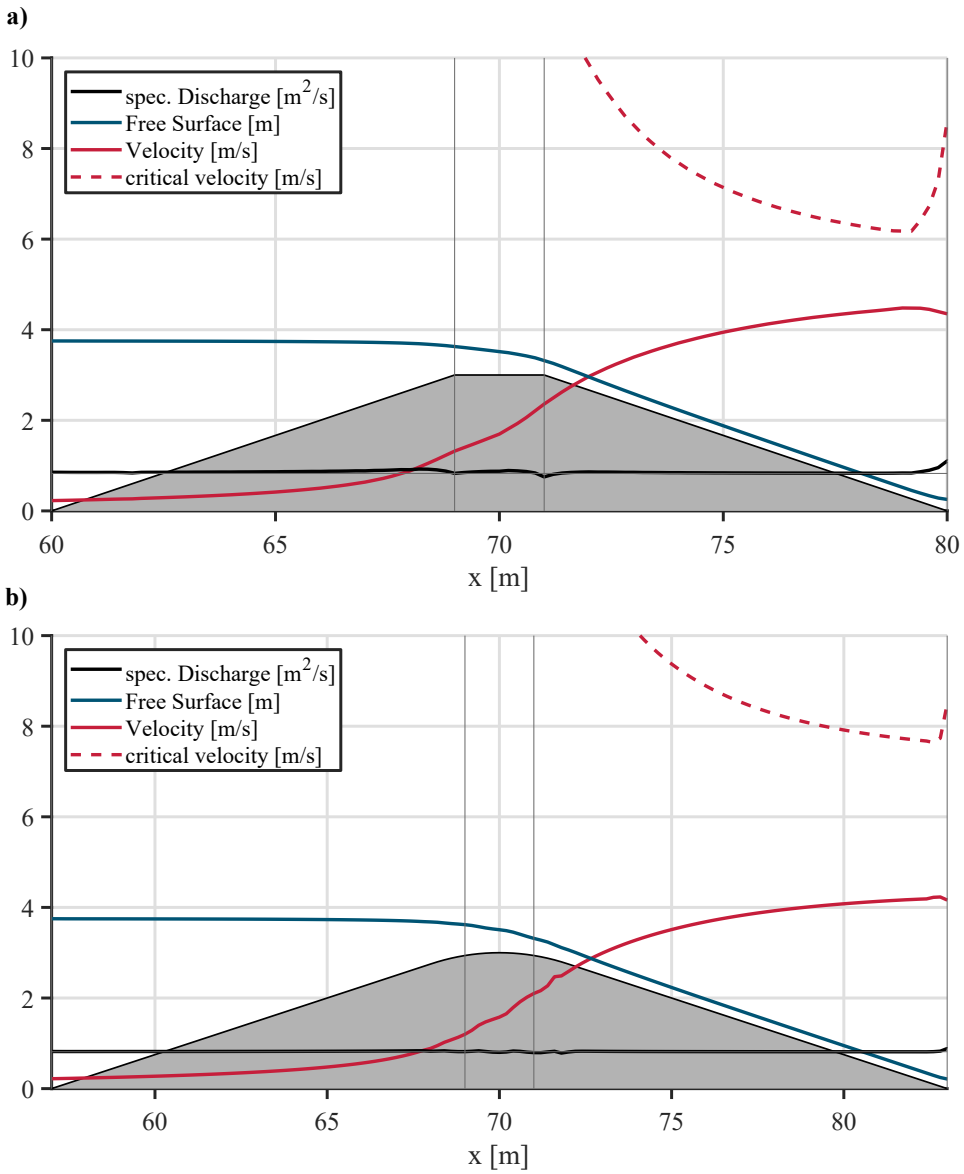

Figure 8: Hydrodynamic parameters at a cross-section of a groin a) with the conventional groin design and b) with an adapted design, including rounding and gentle slopes

efficient model REEF3D::SFLOW, it will lead to significant computation times with the RANSE-based code REEF3D::CFD. Therefore a careful trade-off needs to made for each specific application, if the additional accuracy outweighs the computational effort in employing the REEF3D::CFD module. Experience from dike overtopping due to wind waves suggests that the limited computational demand of depth-averaged software often times outweighs the increased accuracy of high-fidelity models and is usually more applicable for design applications (Lashley et al., 2020).

The simulation of real-scale prototype groins showcases the practical applicability of the solver REEF3D::SFLOW for groin design. This depth-averaged solver was chosen as the interest was restricted to the groin itself, neglecting the hydraulic jump. The required armour layer dimensions obtained by both the Shields equation and the Thornton et al. (2014) equation correspond to observations within field data. Groins constructed with stone classes $CP_{90/250}$, corresponding to $D_{50} = 0.125\,\mathrm{m}$, were damaged in overtopping events in the field. When employing larger rock grading of $LMB_{5/40}$, $D_{50} = 0.22\,\mathrm{m}$ in prototypes, the stability is greatly improved. Independent of the geometric configuration, the required median sieve sizes according to the case study presented are larger than in the previously used grading but smaller than in the adapted grading. The consistency of the numerically and empirically determined armour stone dimensions with the field information, further indicates conceptual validity of the stationary approach.

Numerical data on the influence of groin geometry variations, obtained in the present study, showcases that the required armour layer dimensions are influenced by the groin lee slope. A more gentle slope leads to reduced velocities and also increases armour stone resistance as included in the empirical equations. Here, the Shields equations proves more sensitive to a decrease in slope than the one of Thornton et al.. Using a more gentle wave-facing slope does not affect the required armour layer according to both equations in the studied unidirectional loading. However, a more realistic loading scenario involves ships travelling in both directions. Overtopping events in the reverse direction can hence also be expected. At the same, many ships travel right bound and the drawdown decays with distance to its origin, presumably leading to less damaging overtopping events. However, the dimensional aspect of ship wave loading should be a topic of further research.

A rounding of the groin crest does not reduce the hydrodynamic loading of the groin. However, by implementing this measure, armour stones in the border between crest and slope are less exposed to displacement. This is not reflected within the considered empirical equations; however, other authors, such as Pilarczyk (1995), suggest the use of a stability correction factor to account for armour stones more exposed than when positioned in one continuous layer. Therefore, no final conclusion can be drawn whether a rounding of the crest increases groin stability.

As highlighted in Section primary ship waves exhibit some analogies to tsunami waves. Data on this line of research mostly focuses on the damage occurring to coastal protection structures, such as breakwaters or sea dikes. Damage to the armour layer of the crown and armour layer, similar to the one observed at groins in Elbe estuary (Melling et al., 2019), was one of the eight damage mechanisms qualitatively observed in the experiments of Kato et al. (2012). The authors subjected a trapezoidal sea dike to stationary discharge conditions to mimic the hydraulic loading of a long period tsunami wave. The experiments revealed that at high discharge conditions negative pressure occurred near the dike crown and led to the failure of the armour layer and consequently the washing away of the entire dike.

Quantitative data on armour layer design for rubble mound breakwater armour layer was obtained by Aniel-Quiroga et al. (2018). The authors decomposed the hydrodynamic loading in a solitary wave component and a stationary flow component, that is comparable to the conceptual model of ship wave overtopping. Experimental analysis of scaled breakwaters under the stationary loading situation indicates the danger of an eroding lee slope due to stationary discharge conditions. According to their

results the intensity of erosion mainly depends upon the overflow height. The authors therefore suggest a dimensional analysis based on Hudson's stability number N_S:

$$N_S = \frac{H_{st}}{\Delta D_{n50}}, \tag{12}$$

including the wave height H_{st}, the relative buoyant density Δ, and the nominal stone diameter D_{n50}.

The equation was initially intended for breakwater design under wind waves, such that it is not validated for stationary overtopping situations. As to the different geometry of the examined breakwater (Downstream/landward slope 1:1.5) and the higher water level on the downstream/landward side of the structure the results are further not directly comparable. However, in order to get an estimate of the recommended armour layer dimensions, according to the experimentally determined critical stability number of $N_S = 1.158$ (Aniel-Quiroga et al., 2018) required armour layer dimensions were recalculated for the input parameters relevant to groin design, yielding a value of $D_{n50} = 0.24\,\mathrm{m}$, corresponding to a median sieve size $D_{50} = 0.208$ (BAW, 2010). This value is higher then the ones resulting from the numerical simulations in the present study, which can be explained by the steeper slopes for breakwaters making larger armour layer dimensions necessary. Still, the orders of magnitude for the required stone dimensions agree, therefore indicating the plausibility of the approximated ship wave loads. In addition, the possible information transfer from tsunami research on the prediction of ship waves is emphasized.

For future work several additional points need to be considered. The accuracy of the numerical simulations is reliably backed-up by the experimental validation presented in this study. Yet, the transfer from the hydrodynamic process calculation to the stability information involves a number of parameters that are not fully examined for the application to groins. Both empirical equations include a range of parameters, where one value was chosen from an interval of possible assumptions. The appropriate choice needs to be further examined on basis on experimental and field data.

The stationary loading situation examined in this study is only a sub-set of the ship generated loading conditions. It neglects the additional impact due to the ship-generated wave impact. At the same time, the assumption includes free outflow conditions, corresponding to the theoretically highest ship induced drawdown. Taking into account the stern wave would increase the required armour layer dimensions, while a higher water level in the downstream groin field would potentially decrease the hydraulic loading. Therefore, additional studies are required to determine absolute armour layers with a high level of fidelity, overcoming the introduced assumptions.

The presented application further relies on field data for the determination of critical boundary conditions that lead to damaging effects. The corresponding data is not available at all sites and detailed measurement campaigns for specific sites are costly. Therefore numerical methods are required that determine the water level over time, dependent on ship and waterway parameters, including shallow water deformation processes. With this information at hand, boundary conditions for detailed simulations in the near-field of a groin can be calculated, allowing site specific groin design. With a coupled numerical tool employing REEF3D::SFLOW in the far field and REEF3D::CFD in the near field of groins, time dependent calculations of overtopping events become possible, overcoming the assumption of a stationary flow situation. In addition, more complex geometric configurations can then be incorporated without requiring further measurement campaigns.

Conclusions

This paper presents methods and validation data for the design of rock river groins (spur dikes) to resist ship-induced overtopping events. The frequency and severity of overtopping events increases as average and maximum ship dimensions and the traffic density are increasing. To date, ship waves are not routinely considered in the design of river groins. This study for the first time presents, in principle, a methodology to determine design parameters from numerical simulations. In this paper, we consider a sub-set of the real world loading situation consisting of stationary overflow conditions, induced by ship-induced water-level gradients in adjacent groin fields. In the future, this scenario will be part of a coupled simulation of REEF3D::SFLOW and REEF3D::CFD, allowing a holistic calculation of ship-wave generation, propagation, and wave-structure interaction near the banks.

The study consists of two parts. First, the validation of the hydrodynamic solvers REEF3D::CFD and REEF3D::SFLOW is presented. This is necessary, as ship-induced overtopping is characterized by small hydraulic heads at the upstream side of a groin. Second, the application of the validated solver REEF3D::SFLOW to realistic groin geometries is shown, relying on input from available field data. Required armour layer dimensions are determined, making use of the assumed stationary flow conditions and the critical shear concept of Shields and an empirical equation by Thornton et al. (2014). A parameter study evaluating the effect of different groin geometry was performed. The conclusions from this study are threefold:

- **Validation** Both models are able to predict the relation of discharge and water level reliably. The relation is important to determine the hydrodynamic loading during ship-induced groin overtopping, as this process is governed by different water levels on both sides of a groin. The error margin of the REEF3D::CFD module is smaller than the one of REEF3D::SFLOW. Yet, both models are within an acceptable range of a MAPE below 7 %. The validated codes therefore establish a high level of confidence for future coupled simulations.

- **Application** An application of the validated models on prototype geometries indicates a plausible prediction of the induced loading for critical ship passage events on basis of the assumption of stationary overtopping and empirical equations for the dimensioning of armour stones. The required armour layer dimensions correspond to field observations on damaging events, which further establishes confidence in the numerical approach presented and the description of the damage mechanism in form of a stationary loading situation.

- **Sensitivity of groin geometry** Experiences from prototype design of groins suggest that the reduction of slope angles and smoothing of the groin crest reduce the damage of groins due to ship-generated primary waves. The combination of numerical simulations with empirical equations confirms that a more gentle groin lee slope reduces the necessary armour layer dimensions. A more gentle wave-facing slope has no impact on the required dimensioning in a unidirectional loading scenario. Similarly, rounding the groin crest, has no impact on the hydrodynamic loading of the groin. However, it is suspected that armour layer stability is increased in this case – an effect not taken into account within the considered empirical equations.

A convergence study

The convergence study was realized, following an approach suggested by Viola et al. (2013). With both models, REEF3D::SFLOW and REEF3D::CFD, simulations of the test case at different mesh resolutions were performed. The resulting water level at gauge 1 was examined for all these resolutions. In Figure 9 and 10 the respective grid sizes given at the abscissa are normalized with the reference mesh-resolution ($dx = 1$ cm for SFLOW and $dx = 0.25$ cm for CFD) and the respective water levels given at the ordinate are normalized with the water level at the reference mesh resolution. Grid uncertainty is then calculated from the quality of the fit through the given points and the extrapolated water level at infinitesimally small mesh resolution.

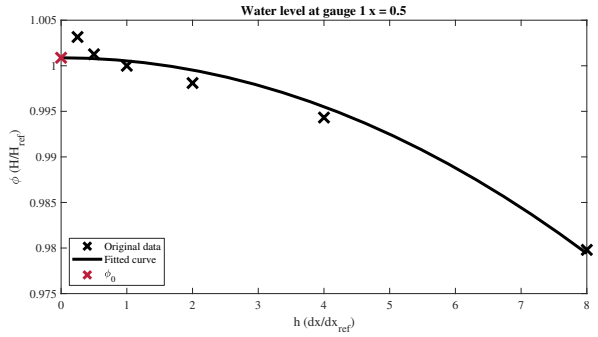

Figure 9: Convergence study for REEF3D::SFLOW based on case #1 and the waterlevel at gauge 1.

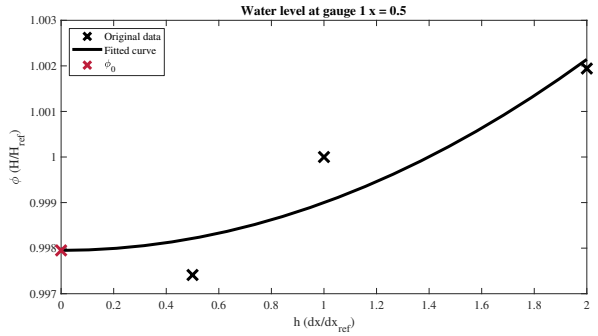

Figure 10: Convergence study for REEF3D::CFD based on case #1 and the waterlevel at gauge 1.

B Identification of stationary state

To identify the stationary state in the simulations, the time history at each gauge of the respective simulations was analyzed. An example time series is given in Figure 11. The respective simulation was then considered to have reached the stationary flow conditions, as soon as the water level at each gauge fluctuated with a standard deviation below 0.001 m.

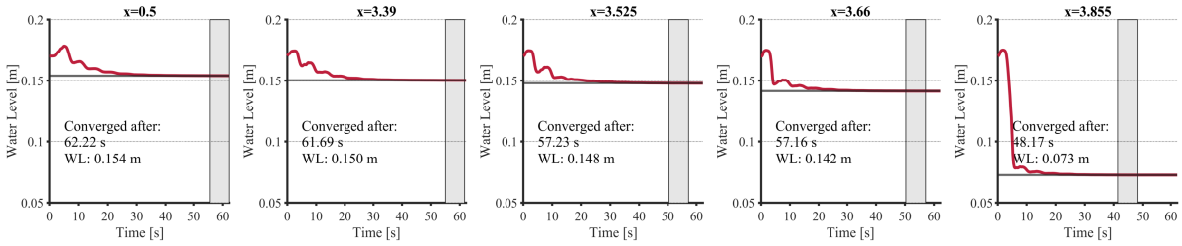

Figure 11: Timeseries of water level development at the gauge locations and the respective time when stationary conditions are setting in each gauge.

APPENDIX III. NOTATION

$\bar{p}$	Depth-averaged dynamic pressure
$\bar{u}, \bar{v}, \bar{w}$	Depth averaged velocity components in x,y,z-direction.
β	Slope angle
ν	Viscosity
ν_t	Turbulent viscosity
ψ	Angle of repose
ρ	Fluid density.
ρ_s	Stone density.
ζ	Free surface elevation
c	Shallow water wave celerity.
C_u	Coefficient of uniformity
d	Still water depth.
D_{50}	Median sieve size
D_{n50}	Nominal stone diameter
dx	Cell size of computational grid
g	Gravitational acceleration (9.81 m/s).
h	Hydraulic head
h_p	Waterlevel at cell center
Hst	Wave height
k_s	Nikuradse roughness length

k_s Slope reduction factor

N Number of samples

N_S Stability number

p Pressure.

p_g Groin height

q Specific discharge

R_m Experimentally obtained value

S Construction slope

T Armour layer thickness

t Time

x_i, x, y, z Coordinates.

APPENDIX IV. ACRONYMS

CFL Courant-Friedrich-Levy.

MAPE Mean Absolute Percentage Error.

MPI Message Passing Interface.

RANSE Reynolds-averaged Navier-Stokes equations.

SWE Shallow-Water-Equations.

Data Availability Statement

All data, models, or code that support the findings of this study are available from the corresponding author upon reasonable request.

Acknowledgments

This study is part of the research project NumSiSSI (Numerical Simulation of Shipwave-Structure-Interaction in Coastal Areas) conducted in cooperation with the German Federal Waterways Engineering and Research Institute (BAW).

References

Afzal, M.S., Bihs, H. and Kumar, L. (2020). Computational fluid dynamics modeling of abutment scour under steady current using the level set method. *International Journal of Sediment Research*, **35**(4), 355–364. ISSN 10016279. doi:10.1016/j.ijsrc.2020.03.003.

Aggarwal, A., Tomaselli, P.D., Christensen, E.D. and Bihs, H. (2020). Computational Fluid Dynamics Investigations of Breaking Focused Wave-Induced Loads on a Monopile and the Effect of Breaker Location. *Journal of Offshore Mechanics and Arctic Engineering*, **142**(2), 021903. ISSN 0892-7219, 1528-896X. doi:10.1115/1.4045187.

Ahmad, N., Bihs, H., Myrhaug, D., Kamath, A. and Arntsen, Ø.A. (2019). Numerical modelling of pipeline scour under the combined action of waves and current with free-surface capturing. *Coastal Engineering*, **148**, 19–35. ISSN 03783839. doi:10.1016/j.coastaleng.2019.02.008.

Alauddin, M., Hossain, M., Uddin, M. and Haque, M. (2017). A review on hydraulic and morphological characteristics in river channels due to spurs. *World Academy of Science, Engineering and Technology International Journal of Geological and Environmental Engineering*, **11**(4), 397–404.

Alauddin, M. and Tsujimoto, T. (2012). Optimum configuration of groynes for stabilization of alluvial rivers with fine sediments. *International Journal of Sediment Research*, **27**(2), 158–167. ISSN 10016279. doi:10.1016/S1001-6279(12)60024-9.

Almström, B., Roelvink, D. and Larson, M. (2021). Predicting ship waves in sheltered waterways – An application of XBeach to the Stockholm Archipelago, Sweden. *Coastal Engineering*, **170**, 104026. ISSN 0378-3839. doi:10.1016/j.coastaleng.2021.104026.

Aniel-Quiroga, Í., Vidal, C., Lara, J., González, M. and Sainz, Á. (2018). Stability of rubble-mound breakwaters under tsunami first impact and overflow based on laboratory experiments. *Coastal Engineering*, **135**, 39–54. ISSN 0378-3839. doi:10.1016/j.coastaleng.2018.01.004.

Arnell, N.W. (1999). The effect of climate change on hydrological regimes in Europe: A continental perspective. *Global Environmental Change*, **9**(1), 5–23. ISSN 09593780. doi:10.1016/S0959-3780(98)00015-6.

BAW (2010). Principles for the design of bank and bottom protection for inland waterways (GBB). Technical report, BAW.

BAW (2018). Schiffserzeugte langperiodische Belastung zur Bemessung der Deckschichten von Strombauwerken an Seeschifffahrtsstraßen. FuE-Abschlussbericht B3955.02.04.70141. Report, Karlsruhe.

Bertram, V. (2012). Resistance and Propulsion. In: *Practical Ship Hydrodynamics*, 73–141. Elsevier. ISBN 978-0-08-097150-6. doi:10.1016/B978-0-08-097150-6.10003-X.

Bhowmik, N.G., Demissie, M. and Osakada, S. (1981). Waves and drawdown generated by river traffic on the Illinois and Mississippi Rivers. Technical report, Illinois State Water Survey.

Bigham, K.A. (2020). Streambank Stabilization Design, Research, and Monitoring: The Current State and Future Needs. *Transactions of the ASABE*, **63**(2), 351–387. ISSN 2151-0040. doi: 10.13031/trans.13647.

Bihs, H., Kamath, A., Alagan Chella, M., Aggarwal, A. and Arntsen, Ø.A. (2016). A new level set numerical wave tank with improved density interpolation for complex wave hydrodynamics. *Computers & Fluids*, **140**, 191–208. ISSN 00457930. doi:10.1016/j.compfluid.2016.09.012.

Chen, Y., Fu, Z., Chen, Q. and Cui, Z. (2018). Discharge Coefficient of Rectangular Short-Crested Weir with Varying Slope Coefficients. *Water*, **10**(2), 204. ISSN 2073-4441. doi:10.3390/w10020204.

CIRIA (Editor) (2007). *The Rock Manual - the Use of Rock in Hydraulic Engineering*. CIRIA, London, 2. ed edition. ISBN 978-0-86017-683-1.

Darvishi, E., Fenton, J.D. and Kouchakzadeh, S. (2017). Boussinesq equations for flows over steep slopes and structures. *Journal of Hydraulic Research*, **55**(3), 324–337. ISSN 0022-1686. doi: 10.1080/00221686.2016.1246484.

David, C.G., Roeber, V., Goseberg, N. and Schlurmann, T. (2017). Generation and propagation of ship-borne waves - Solutions from a Boussinesq-type model. *Coastal Engineering*, **127**, 170–187. ISSN 03783839. doi:10.1016/j.coastaleng.2017.07.001.

Dempwolff, L.C., Martin, T., Windt, C., Melling, G., Bihs, H. and Goseberg, N. (2022*a*). Computational Methods for Wave Structure Interaction Modelling in Coastal Environments Under Consideration of Bathymetric Attributes. *Proceedings of the ASME 41st International Conference on Ocean, Offshore and Arctic Engineering 2022, Hamburg, Germany*.

Dempwolff, L.C., Melling, G., Windt, C., Lojek, O., Martin, T., Holzwarth, I., Bihs, H. and Goseberg, N. (2022*b*). Loads and effects of ship-generated, drawdown waves in confined waterways - A review of current knowledge and methods. *Journal of Coastal and Hydraulic Structures*, **2**, 46. ISSN 2667-047X. doi:10.48438/jchs.2022.0013.

Didenkulova, I., Pelinovsky, E. and Soomere, T. (2011). Can the Waves Generated by Fast Ferries be a Physical Model of Tsunami? *Pure and Applied Geophysics*, **168**(11), 2071–2082. ISSN 0033-4553, 1420-9136. doi:10.1007/s00024-011-0289-z.

Elsayed, S.M., Gijsman, R., Schlurmann, T. and Goseberg, N. (2022). Nonhydrostatic Numerical Modeling of Fixed and Mobile Barred Beaches: Limitations of Depth-Averaged Wave Resolving Models around Sandbars. *Journal of Waterway, Port, Coastal, and Ocean Engineering*, **148**(1), 04021045. ISSN 0733-950X, 1943-5460. doi:10.1061/(ASCE)WW.1943-5460.0000685.

Engelhardt, C., Krüger, A., Sukhodolov, A. and Nicklisch, A. (2004). A study of phytoplankton spatial distributions, flow structure and characteristics of mixing in a river reach with groynes. *Journal of Plankton Research*, **26**(11), 1351–1366. ISSN 0142-7873. doi:10.1093/plankt/fbh125.

EurOtop (2018). *Manual on Wave Overtopping of Sea Defences and Related Structures. An Overtopping Manual Largely Based on European Research, but for Worldwide Application*. Van der Meer, J.W., Allsop, N.W.H., Bruce, T., De Rouck, J., Kortenhaus, A., Pullen, T., Schüttrumpf, H., Troch, P. and Zanuttigh, B.

Finkl, C.W. and Makowski, C. (Editors) (2019). *Encyclopedia of Coastal Science*. Encyclopedia of Earth Sciences Series. Springer International Publishing, Cham. ISBN 978-3-319-93805-9 978-3-319-93806-6. doi:10.1007/978-3-319-93806-6.

Forlini, C., Qayyum, R., Malej, M., Lam, M.A.Y.H., Shi, F., Angelini, C. and Sheremet, A. (2021). On the Problem of Modeling the Boat Wake Climate: The Florida Intracoastal Waterway. *Journal of Geophysical Research: Oceans*, **126**(2). ISSN 2169-9275, 2169-9291. doi:10.1029/2020JC016676.

Garde, R.J., Subramanya, K. and Nambudripad, K.D. (1961). Study of Scour Around Spur-Dikes. *Journal of the Hydraulics Division*, **87**(6), 23–37. ISSN 0044-796X, 2690-2524. doi:10.1061/JYCEAJ.0000663.

Goseberg, N. (2013). Reduction of maximum tsunami run-up due to the interaction with beachfront development – application of single sinusoidal waves. *Natural Hazards and Earth System Sciences*, **13**(11), 2991–3010. ISSN 1684-9981. doi:10.5194/nhess-13-2991-2013.

Gourlay, T.P. (2001). The supercritical bore produced by a high-speed ship in a channel. *Journal of Fluid Mechanics*, **434**, 399–409. ISSN 0022-1120, 1469-7645. doi:10.1017/S002211200100372X.

Habersack, H. and Nachtnebel, H.P. (1995). Short-term effects of local river restoration on morphology, flow field, substrate and biota. *Regulated Rivers: Research & Management*, **10**(2-4), 291–301. ISSN 08869375, 10991646. doi:10.1002/rrr.3450100222.

Hager, W.H. (1987). Lateral Outflow Over Side Weirs. *Journal of Hydraulic Engineering*, **113**(4), 491–504. ISSN 0733-9429, 1943-7900. doi:10.1061/(ASCE)0733-9429(1987)113:4(491).

Han, J., Sun, Z., Li, Y. and Yang, Y. (2017). Combined effects of multiple large-scale hydraulic engineering on water stages in the middle Yangtze River. *Geomorphology*, **298**, 31–40. ISSN 0169555X. doi:10.1016/j.geomorph.2017.09.034.

Haun, S., Olsen, N.R.B. and Feurich, R. (2011). Numerical Modeling of Flow Over Trapezoidal Broad-Crested Weir. *Engineering Applications of Computational Fluid Mechanics*, **5**(3), 397–405. ISSN 1994-2060, 1997-003X. doi:10.1080/19942060.2011.11015381.

Hirabayashi, Y., Mahendran, R., Koirala, S., Konoshima, L., Yamazaki, D., Watanabe, S., Kim, H. and Kanae, S. (2013). Global flood risk under climate change. *Nature Climate Change*, **3**(9), 816–821. ISSN 1758-678X, 1758-6798. doi:10.1038/nclimate1911.

Hudson, R.Y. (1959). Laboratory investigation of rubble-mound breakwaters. *Journal of the waterways and Harbors division*, **85**(3), 93–121.

Hughes, S.A. (1993). *Physical Models and Laboratory Techniques in Coastal Engineering*, volume 7. World Scientific.

Hughes, S.A. and Nadal, N.C. (2009). Laboratory study of combined wave overtopping and storm surge overflow of a levee. *Coastal Engineering*, **56**(3), 244–259. ISSN 0378-3839. doi:10.1016/j.coastaleng.2008.09.005.

Huthoff, F., Pinter, N. and Remo, J.W.F. (2013). Theoretical Analysis of Wing Dike Impact on River Flood Stages. *Journal of Hydraulic Engineering*, **139**(5), 550–556. ISSN 0733-9429, 1943-7900. doi:10.1061/(ASCE)HY.1943-7900.0000698.

Jeschke, A., Pedersen, G.K., Vater, S. and Behrens, J. (2017). Depth-averaged non-hydrostatic extension for shallow water equations with quadratic vertical pressure profile: Equivalence to Boussinesq-type equations. *International Journal for Numerical Methods in Fluids*, **84**(10), 569–583. ISSN 02712091. doi:10.1002/fld.4361.

Jiang, L., Diao, M., Sun, H. and Ren, Y. (2018). Numerical Modeling of Flow Over a Rectangular Broad-Crested Weir with a Sloped Upstream Face. *Water*, **10**(11), 1663. doi:10.3390/w10111663.

Kamath, A., Alagan Chella, M., Bihs, H. and Arntsen, Ø.A. (2017). Energy transfer due to shoaling and decomposition of breaking and non-breaking waves over a submerged bar. *Engineering Applications of Computational Fluid Mechanics*, **11**(1), 450–466. ISSN 1994-2060, 1997-003X. doi:10.1080/19942060.2017.1310671.

Kamath, A., Fleit, G. and Bihs, H. (2019). Investigation of Free Surface Turbulence Damping in RANS Simulations for Complex Free Surface Flows. *Water*, **11**(3), 456. ISSN 2073-4441. doi:10.3390/w11030456.

Kato, F., Suwa, Y., Watanabe, K. and Hatogai, S. (2012). Mechanisms of coastal dike failure induced by the great east japan earthquake tsunami. *Coastal Engineering Proceedings*, **1**(33), 40. ISSN 2156-1028, 0589-087X. doi:10.9753/icce.v33.structures.40.

Kuhnle, R., Alonso, C. and Shields Jr., F. (2002). Local scour associated with angled spur dikes. *Journal of Hydraulic Engineering*, **128**(12), 1087–1093. ISSN 0733-9429. doi:10.1061/(ASCE)0733-9429(2002)128:12(1087).

Labat, D., Goddéris, Y., Probst, J. and Guyot, J. (2004). Evidence for global runoff increase related to climate warming. *Advances in Water Resources*, **27**(6), 631–642. ISSN 0309-1708. doi:10.1016/j.advwatres.2004.02.020.

Lashley, C.H., Zanuttigh, B., Bricker, J.D., van der Meer, J., Altomare, C., Suzuki, T., Roeber, V. and Oosterlo, P. (2020). Benchmarking of numerical models for wave overtopping at dikes with shallow mildly sloping foreshores: Accuracy versus speed. *Environmental Modelling & Software*, **130**, 104740. ISSN 13648152. doi:10.1016/j.envsoft.2020.104740.

Lataire, E. and Vantorre, M. (2008). Ship-Bank Interaction Induced by Irregular Bank Geometries. *Proceedings of the 27th Symposium on Naval Hydrodynamics*.

Martin, T., Kamath, A. and Bihs, H. (2020). Modeling and Simulation of Moored-Floating Structures Using the Tension Element Method. *Journal of Offshore Mechanics and Arctic Engineering*, **142**(1), 011803. ISSN 0892-7219, 1528-896X. doi:10.1115/1.4044289.

Martin, T., Tsarau, A. and Bihs, H. (2021). A numerical framework for modelling the dynamics of open ocean aquaculture structures in viscous fluids. *Applied Ocean Research*, **106**, 102410. ISSN 01411187. doi:10.1016/j.apor.2020.102410.

McCoy, A., Constantinescu, G. and Weber, L.J. (2008). Numerical Investigation of Flow Hydrodynamics in a Channel with a Series of Groynes. *Journal of Hydraulic Engineering*, **134**(2), 157–172. ISSN 0733-9429, 1943-7900. doi:10.1061/(ASCE)0733-9429(2008)134:2(157).

Méhauté, B. (1976). *An Introduction to Hydrodynamics and Water Waves*. Springer, Berlin, Heidelberg. ISBN 978-3-642-85569-6 978-3-642-85567-2. doi:10.1007/978-3-642-85567-2.

Melling, G., Jansch, H., Kondziella, B., Uliczka, K. and Gätje, B. (2019). Damage to Rock Groynes from Long-Period Ship Waves: Towards a Probabilistic Design Method. *Proceedings of the Coastal Structures Conference 2019, Hannover, Germany*. doi:10.18451/978-3-939230-64-9_002.

Melling, G., Jansch, H., Kondziella, B., Uliczka, K. and Gätje, B. (2020). Evaluation of optimised groyne designs in response to long-period ship wave loads at Juelssand in the Lower Elbe Estuary. *Die Küste*, **89**, 28. ISSN 0452-7739. doi:10.18171/1.089103.

Microsonic (2022). Mic+35/IU/TC | Ultraschallsensor. https://www.microsonic.de/de/abstandssensoren/zylindrisch/micplu

Minor, B., Rennie, C.D. and Townsend, R.D. (2007). "Barbs" for river bend bank protection: Application of a three-dimensional numerical model. *Canadian Journal of Civil Engineering*, **34**(9), 1087–1095. ISSN 0315-1468, 1208-6029. doi:10.1139/l07-088.

Nijssen, B., O'donnell, G., Hamlet, A. and Lettenmaier, D. (2001). Hydrologic sensitivity of global rivers to climate change. *Climatic Change*, **50**(1-2), 143–175. ISSN 0165-0009. doi:10.1023/A:1010616428763.

Pandey, M., Ahmad, Z. and Sharma, P. (2016). Estimation of maximum scour depth near a spur dike. *Canadian Journal of Civil Engineering*, **43**(3), 270–278. ISSN 0315-1468, 1208-6029. doi:10.1139/cjce-2015-0280.

Pilarczyk, K. (1995). Simplified unification of stability formulae for revetments under current and wave attack. *River, Coastal, and Shoreline Protection: Erosion Control Using Riprap and Armourstone*, 53–73.

Przedwojski, B. (1995). Bed topography and local scour in rivers with banks protected by groynes. *Journal of Hydraulic Research*, **33**(2), 257–273. ISSN 0022-1686, 1814-2079. doi:10.1080/00221689509498674.

Rahman, M. and Muramoto, Y. (1999). Prediction of maximum scour depth around spur-dike-like structures. *Proceedings of hydraulic engineering*, **43**, 623–628.

Remo, J.W., Pinter, N. and Heine, R. (2009). The use of retro- and scenario-modeling to assess effects of 100+ years river of engineering and land-cover change on Middle and Lower Mississippi River flood stages. *Journal of Hydrology*, **376**(3-4), 403–416. ISSN 00221694. doi:10.1016/j.jhydrol.2009.07.049.

Říha, J., Duchan, D., Zachoval, Z., Erpicum, S., Archambeau, P., Pirotton, M. and Dewals, B. (2019). Performance of a shallow-water model for simulating flow over trapezoidal broad-crested weirs. *Journal of Hydrology and Hydromechanics*, **67**(4), 322–328. ISSN 0042-790X. doi: 10.2478/johh-2019-0014.

Rodrigues, S., Santos, J. and Guedes Soares, C. (2018). Numerical and experimental study of ship-generated waves. In: *Proceedings of Progress in Maritime Technology and Engineering, Lisbon, Portugal*.

Roelvink, D., Reniers, A., van Dongeren, A., van Thiel de Vries, J., McCall, R. and Lescinski, J. (2009). Modelling storm impacts on beaches, dunes and barrier islands. *Coastal Engineering*, **56**(11-12), 1133–1152. ISSN 03783839. doi:10.1016/j.coastaleng.2009.08.006.

Schwartz, R. and Kozerski, H.P. (2003). Entry and Deposits of Suspended Particulate Matter in Groyne Fields of the Middle Elbe and its Ecological Relevance. *Acta hydrochimica et hydrobiologica*, **31**(4-5), 391–399. ISSN 1521-401X. doi:10.1002/aheh.200300496.

Sharp, J.A. and McAnally, W.H. (2012). Numerical modeling of surge overtopping of a levee. *Applied Mathematical Modelling*, **36**(4), 1359–1370. ISSN 0307904X. doi:10.1016/j.apm.2011.08.039.

Shi, F., Malej, M., Smith, J.M. and Kirby, J.T. (2018). Breaking of ship bores in a Boussinesq-type ship-wake model. *Coastal Engineering*, **132**, 1–12. ISSN 03783839. doi:10.1016/j.coastaleng. 2017.11.002.

Shields, A. (1936). Anwendung der Aehnlichkeitsmechanik und der Turbulenzforschung auf die Geschiebebewegung. Ph.D. thesis Technical University Berlin, Preussische Versuchsanstalt für Wasserbau.

Silinski, A., Heuner, M., Schoelynck, J., Puijalon, S., Schröder, U., Fuchs, E., Troch, P., Bouma, T.J., Meire, P. and Temmerman, S. (2015). Effects of Wind Waves versus Ship Waves on Tidal Marsh Plants: A Flume Study on Different Life Stages of Scirpus maritimus. *PLOS ONE*, **10**(3), e0118687. ISSN 1932-6203. doi:10.1371/journal.pone.0118687.

Sukhodolov, A., Engelhardt, C., Krüger, A. and Bungartz, H. (2004). Case Study: Turbulent Flow and Sediment Distributions in a Groyne Field. *Journal of Hydraulic Engineering*, **130**(1), 1–9. ISSN 0733-9429, 1943-7900. doi:10.1061/(ASCE)0733-9429(2004)130:1(1).

Sukhodolov, A.N. (2014). Hydrodynamics of groyne fields in a straight river reach: Insight from field experiments. *Journal of Hydraulic Research*, **52**(1), 105–120. ISSN 0022-1686, 1814-2079. doi:10.1080/00221686.2014.880859.

Thornton, C.I., Abt, S.R., Scholl, B.N. and Bender, T.R. (2014). Enhanced Stone Sizing for Overtopping Flow. *Journal of Hydraulic Engineering*, **140**(4), 06014005. ISSN 0733-9429, 1943-7900. doi: 10.1061/(ASCE)HY.1943-7900.0000830.

Tingsanchali, T. and Maheswaran, S. (1990). 2-D Depth-Averaged Flow Computation near Groyne. *Journal of Hydraulic Engineering*, **116**(1), 71–86. ISSN 0733-9429, 1943-7900. doi:10.1061/ (ASCE)0733-9429(1990)116:1(71).

Tomiczek, T., Wargula, A., O'Donnell, K., LaVeck, V., Castagno, K.A. and Scyphers, S. (2022). Vessel-Generated Wake Attenuation by *Rhizophora Mangle* in Key West, Florida. *Journal of Waterway, Port, Coastal, and Ocean Engineering*, **148**(3), 04022002. ISSN 0733-950X, 1943-5460. doi:10.1061/(ASCE)WW.1943-5460.0000704.

Uijttewaal, W.S. (2005*a*). Effects of Groyne Layout on the Flow in Groyne Fields: Laboratory Experiments. *Journal of Hydraulic Engineering*, **131**(9), 782–791. ISSN 0733-9429, 1943-7900. doi:10.1061/(ASCE)0733-9429(2005)131:9(782).

Uijttewaal, W.S. (2005*b*). The flow in groyne fields. In: *Water Quality Hazards and Dispersion of Pollutants*, 231–246. Springer.

Uijttewaal, W.S.J., Lehmann, D. and van Mazijk, A. (2001). Exchange Processes between a River and Its Groyne Fields: Model Experiments. *Journal of Hydraulic Engineering*, **127**(11), 928–936. ISSN 0733-9429, 1943-7900. doi:10.1061/(ASCE)0733-9429(2001)127:11(928).

van der Meer, J. (1987). Stability of breakwater armour layers — design formulae. *Coastal Engineering*, **11**, 219–239.

Van Gent, M.R.A., Smale, A.J. and Kuiper, C. (2004). Stability of Rock Slopes with Shallow Foreshores. In: *In the Proceedings of: Coastal Structures 2003*, 100–112. American Society of Civil Engineers. doi:10.1061/40733(147)9.

van Stokkom, H.T., Smits, A.J. and Leuven, R.S. (2005). Flood Defense in The Netherlands: A New Era, a New Approach. *Water International*, **30**(1), 76–87. ISSN 0250-8060, 1941-1707. doi:10.1080/02508060508691839.

Vanden-Broeck, J.M. and Keller, J.B. (1987). Weir flows. *Journal of Fluid Mechanics*, **176**(-1), 283. ISSN 0022-1120, 1469-7645. doi:10.1017/S0022112087000673.

Viola, I., Bot, P. and Riotte, M. (2013). On the uncertainty of CFD in sail aerodynamics. *International Journal for Numerical Methods in Fluids*, **72**(11), 1146–1164. ISSN 02712091. doi:10.1002/fld.3780.

Vischer, D. and Huber, A. (2002). Schutzwasserbauten. In: *Wasserbau: Hydrologische Grundlagen, Elemente Des Wasserbaus, Nutz- Und Schutzbauten an Binnengewässern*, 282–345. Springer Berlin Heidelberg, Berlin, Heidelberg. ISBN 978-3-662-10852-9. doi:10.1007/978-3-662-10852-9âĆĄ0.

von Häfen, H., Goseberg, N., Stolle, J. and Nistor, I. (2019). Gate-Opening Criteria for Generating Dam-Break Waves. *Journal of Hydraulic Engineering*, **145**(3), 04019002. ISSN 0733-9429, 1943-7900. doi:10.1061/(ASCE)HY.1943-7900.0001567.

Wang, W., Kamath, A., Martin, T., Pákozdi, C. and Bihs, H. (2020*a*). A Comparison of Different Wave Modelling Techniques in An Open-Source Hydrodynamic Framework. *Journal of Marine Science and Engineering*, **8**(7), 526. ISSN 2077-1312. doi:10.3390/jmse8070526.

Wang, W., Martin, T., Kamath, A. and Bihs, H. (2020*b*). An improved depth-averaged nonhydrostatic shallow water model with quadratic pressure approximation. *International Journal for Numerical Methods in Fluids*, **92**(8), 803–824. ISSN 0271-2091, 1097-0363. doi:10.1002/fld.4807.

Weitbrecht, V., Socolofsky, S.A. and Jirka, G.H. (2008). Experiments on Mass Exchange between Groin Fields and Main Stream in Rivers. *Journal of Hydraulic Engineering*, **134**(2), 173–183. ISSN 0733-9429, 1943-7900. doi:10.1061/(ASCE)0733-9429(2008)134:2(173).

Wöffler, T., Gier, F. and Schüttrumpf, H. (2013). Schiffserzeugte langperiodische Belastung zur Bemessung der Deckschichten von Strombauwerken an Seeschifffahrtsstraßen – Projektskizze Arbeitspaket 4: Kleinmaßstäbliche Untersuchungen zur Erfassung der maßgebenden Prozesse und zur hydraulischen Stabilität. Technical report, Lehrstuhl und Institut für Wasserbau und Wasserwirtschaft, Rheinisch-Westfälische Technische Hochschule Aachen.

WSV (2016). Portal Tideelbe: https://www.kuestendaten.de/Tideelbe/DE/Service/Kartentool/Kartentool_node.html.

Xiang, K., Yang, Z., Wu, S., Gao, W., Li, D. and Li, Q. (2020). Flow hydrodynamics of the mixing layer in consecutive vegetated groyne fields. *Physics of Fluids*, **32**(6), 065110. ISSN 1070-6631, 1089-7666. doi:10.1063/5.0006317.

Zhang, L., Wang, P., Yang, W., Zuo, W., Gu, X. and Yang, X. (2018). Geometric Characteristics of Spur Dike Scour under Clear-Water Scour Conditions. *Water*, **10**(6), 680. ISSN 2073-4441. doi:10.3390/w10060680.

Zijlema, M., Stelling, G. and Smit, P. (2011). SWASH: An operational public domain code for simulating wave fields and rapidly varied flows in coastal waters. *Coastal Engineering*, **58**(10), 992–1012. ISSN 03783839. doi:10.1016/j.coastaleng.2011.05.015.